Received: 22 January 2022 | Accepted: 25 February 2022

DOI: 10.1111/bpa.13065

Brain Pathology

RESEARCH ARTICLE

Vascular endothelial growth factor-C modulates cortical NMDA receptor activity in cortical lesions of young patients and rat model with focal cortical dysplasia

Kai-Feng Shen[1] | **Qing-Tian Duan**[1] | **Wei Duan**[2] | **Sen-Lin Xu**[3] | **Ning An**[1] | **Yan-Yan Ke**[1] | **Li-Ting Wang**[4] | **Shi-Yong Liu**[1] | **Hui Yang**[1,5] | **Chun-Qing Zhang**[1,5]

[1]Department of Neurosurgery, Epilepsy Research Center of PLA, Xinqiao Hospital, Army Medical University, Chongqing, China

[2]Department of Neurology, Xinqiao Hospital, Army Medical University, Chongqing, China

[3]Institute of Pathology, Southwest Hospital, Army Medical University, Chongqing, China

[4]Biomedical Analysis Center, Army Medical University, Chongqing, China

[5]Guangyang Bay Laboratory, Chongqing Institute for Brain and Intelligence, Chongqing, China

Correspondence
Chun-Qing Zhang, Department of Neurosurgery, Xinqiao Hospital, Army Medical University, 183 Xinqiao Main Street, Chongqing 400037, China.
Email: cqzhang@tmmu.edu.cn

Funding information
Training project of clinical medical researcher of Army Medical University, Grant/Award Number: 2018XLC3046; Chongqing Technology Innovation and Application Development Special key Project, Grant/Award Number: cstc2019jscx-dxwtBX0010; National Natural Science Foundation of China, Grant/Award Number: 81771217 and 81873757; Chongqing Scientific and health Joint medical scientific research project, Grant/Award Number: 2019MSXM099

Abstract

Emergence of dysmorphic neurons is the primary pathology in focal cortical dysplasia (FCD) associated pediatric intractable epilepsy; however, the etiologies related to the development and function of dysmorphic neurons are not fully understood. Our previous studies revealed that the expression of vascular endothelial growth factor-C (VEGF-C) and corresponding receptors VEGFR-2, VEGFR-3 was increased in the epileptic lesions of patients with tuberous sclerosis complex or mesial temporal lobe epilepsy. Here, we showed that the expression of VEGF-C, VEGFR-2, and VEGFR-3 was increased at both mRNA and protein levels in patients with cortical lesions of type I, IIa, and IIb FCD. The immunoreactivity of VEGF-C, VEGFR-2 and VEGFR-3 was located in the micro-columnar neurons in FCD type I lesions, dysplastic neurons (DNs) in FCD type IIa lesions, balloon cells (BCs) and astrocytes in FCD type IIb lesions. Additionally, the amplitude of evoked-EPSCs (eEPSC) mediated by NMDA receptor, the ratio of NMDA receptor- and AMPA receptor-mediated eEPSC were increased in the dysmorphic neurons of FCD rats established by prenatal X-ray radiation. Furthermore, NMDA receptor mediated current in dysmorphic neurons was further potentiated by exogenous administration of VEGF-C, however, could be antagonized by ki8751, the blocker of VEGFR-2. These results suggest that VEGF-C system participate in the pathogenesis of cortical lesions in patients with FCD in association with modulating NMDA receptor–mediated currents.

KEYWORDS
focal cortical dysplasia, NMDA receptor, vascular endothelial growth factor receptor-C, vascular endothelial growth factor 2 and 3

Kai-Feng Shen and Qing-Tian Duan contributed equally to this work.

1 | INTRODUCTION

Focal cortical dysplasia (FCD) is a specific cortical malformation occurred during the development and represents the most prevalent etiology of medically intractable epilepsy in children, leading to surgical resection of the lesions or neurostimulation treatment ultimately [1, 2]. FCD is classified into type I and type II according to the current international consensus classification by ILAE [3]. Type I FCD is characterized histologically with dyslamination of the neocortex (the presence of microcolumns), and Type II is characterized by cortical dyslamination and dysplastic neurons (DNs) with (Type IIb) or without balloon cells (BCs) (Type IIa) [4]. Previous studies have revealed that dysmorphic neurons in FCD lesions are the potential generator of seizure discharges [5, 6]; however, specific mechanisms governing the development of hyperexcitability in the dysmorphic neurons are not well known.

Vascular endothelial growth factors C (VEGF-C) is a member of the VEGF family and acts as a neurotrophic factor in the nervous system by regulating biological events such as angiogenesis, vasculogenesis, and lymphangiogenesis [7–9]. It was reported that VEGF-C promotes neurogenesis and has neuroprotective effects in the central nervous system in several neurological disorders by interacting with specific receptors such as VEGFR-2 (flk-1) and VEGFR-3 (flt-4) [10–14]. Our previous studies revealed that the expression of VEGF-C, VEGFR-2, and VEGFR-3 was increased in the epileptic lesions of patients with tuberous sclerosis complex or mesial temporal lobe epilepsy [15, 16]. However, little is known regarding the role of VEGF-C in the pathogenesis and epileptogenicity of FCD.

N-methyl-D-aspartic acid (NMDA) receptor plays important role in mediating the glutamate-induced excitatory currents. The molecular composition of NMDA receptor was found to be altered in the cortical samples of patients with FCD and relevant animal models [17–19]. However, whether NMDA receptor mediated current is altered in the dysmorphic neurons and with regarding to the potential mechanisms, it is rarely identified.

Here, with brain specimens from patients with FCD and FCD rats generated by in utero X-ray radiation, we detected the expression pattern of VEGF-C, VEGFR-2, and VEGFR-3 in the cortical lesions and investigated the effect of VEGF-C on NMDA receptor-mediated current in the neurons of the dysplastic cortex.

2 | MATERIALS AND METHODS

2.1 | Human brain tissue samples

The study was approved by the Ethics Committee of Army Medical University. FCD-induced pediatric medically refractory epilepsy was diagnosed according to the current international consensus classification proposed by the International League Against Epilepsy (ILAE) [3]. Intraoperative electrocorticography were performed in all the enrolled patients during the operation, and invasive depth electrode recordings were performed if the epileptic lesions could not be precisely located by scalp electroencephalogram before the surgery. All the specimens were obtained from patients with FCD who underwent surgical resection. Only epileptogenic tissues that were identified as dysplastic cortex by magnetic resonance imaging and further confirmed post hoc by neuropathological correction were used in the study. All the procedures and experiments were performed in comply with the Declaration of Helsinki and the guidelines for conduction of research involving human subjects, as established by the Ethics committee of Army Medical University. Informed written consent was obtained from all participants or legal guardians for the use of dissected tissue in research purpose only.

A total of 37 surgical specimens including 12 FCD I (male/female: 7/5; mean age 7.5, range 2.4–15.0), 12 FCD IIa (male/female: 7/5; mean age 6.5, range 2.5–14.5), and 13 FCD IIb (male/female: 7/6; mean age 6.3, range 1.5–13.5) were examined in the present study. The clinical information of patients with FCD is summarized in Table 1. Detailed clinical data for each FCD patient specimen are listed in Table S1. The control cortex (CTX) specimens were obtained from autopsies of 10 age-matched patients (male/female: 5/5; mean age 6.0, range 2.0–12.4) without a history of neurologic diseases, and detailed clinical data were summarized in Table S2. All autopsies were performed within 6 h of death, within which the majority of mRNA and protein are well preserved [20, 21].

All the specimens obtained from surgical resection or autopsies were immediately frozen in liquid nitrogen and then stored at −80°C for Real-time Quantitative PCR (RT-PCR) or Western blot analysis, or fixed in 4% paraformaldehyde (PFA) and then dehydrated in 30% sucrose for in situ hybridization (ISH) or immunohistochemistry/immunofluorescence.

2.2 | Animal studies

Sprague-Dawley rats (*Rattus norvegicus*) were housed under standard conditions (room temperature, 23 ± 1°C; illumination, 12-h light/12-h dark cycle; access to food and water, ad libitum). Randomly chosen female rats were exposed to X-ray (225 cGy, 60 s) (RS-2000, Rad Source Technologies) at post pregnancy day 17 to disrupt the normal development of cortex in utero, and newborns were weaned at postnatal day 21 (P21) after normally delivery according to previous procedure [22, 23]. All the animal experimental procedures were reviewed and approved by the Internal Animal Care and Use Committee of the Army Medical University.

TABLE 1 Summary of the clinical features of patients with FCD

	FCD I (n = 12)	FCD IIa (n = 12)	FCD IIb (n = 13)
Male/female	7/5	7/5	7/6
Mean age of surgery (years)	7.6 (2.4–15)	6.5 (2.5–14.5)	6.3 (1.5–13.5)
Seizure type	PS (75%); GTCS (50%); Tonic (17%); IS (8%)	PS (67%); GTCS (42%); Tonic (17%); IS (17%)	PS (46%); GTCS (69%); Tonic (15%); IS (8%)
Lesions location	Frontal (5); Temporal (4); Parietal (4); Occipital (3)	Frontal (6); Temporal (4); Parietal (3); Occipital (1)	Frontal (8); Temporal (4); Parietal (3); Occipital (3)
Duration of epilepsy (years)	5.2 (1.5–10)	4.9 (1.0–9.0)	4.23 (1.0–8.8)
Seizure frequency (per month)	59.4	72.6	52.9
Postoperative outcome (Engel's class)	I: 42%; II: 33%; III: 25%; IV: 0%	I: 50%; II: 25%; III: 17%; IV: 8%	I: 77%; II: 23%; III: 0; IV: 0

Abbreviations: GTCS, generalized tonic-clonic seizure; IS, infantile spasm; PS, partial seizure.

At 4 weeks of age, the rats exposed to embryonic X-ray were anesthetized with pentobarbital sodium (60 mg/kg) and perfused with 4% PFA to dissect the brain for morphological analysis. HE staining was used to detect the cortical structure and the neuronal morphology in the lesion and identify whether the FCD model was established according to neuropathological criteria [22, 23].

2.3 | RT-PCR

Total RNA was isolated by the Trizol reagent (Invitrogen, Carlsbad, CA) following the manufacture instructions. The RNA concentration and quality were evaluated spectrophotometrically at 260/280 nm (of ratio: 1.9–2.0) with a nanodrop spectrophotometer (Ocean Optics, Dunedin, FL). Single-stranded cDNA was reverse-transcribed from 1 μg total RNA using an oligo dT primer (Takara, Otsu, Japan). Following primers were used for the PCR: VEGF-C (forward: 5′-AGCAAAGATCTGGAGGAGCAG; reverse: 5′-TTATGTTGCCAGCCTCCTTTC), VEGFR-2 (forward: 5′-AAAGTGATCGGAAATGACAC; reverse: 5′-GGAATCACCACAGTTTTGTT), VEGFR-3 (forward: 5′-TTACAACTGGGTGTCCTTTC; reverse: 5′-TTCTTGTCTATGCCTGCTCT), and GAPDH (forward: 5′-ACGGATTTGGTCGTATTGGG; reverse: 5′-TGATTTTGGAGGGATCTCGC). The PCR cycle was set as follows: 95°C for 3 min (one cycle), followed by 40 PCR cycles of denaturation at 95°C for 40 s, 40 s of annealing at 58°C, and 30 s of extension at 72°C. GAPDH was used as internal control. Each quantitative PCR reaction was repeated for at least three times, and the whole RT-PCR analyses were repeated by least two independent experiments. The PCR products were relatively quantified by the $2^{-\triangle\triangle ct}$ method against the internal control (GAPDH).

2.4 | Western blot

Protein was extracted by homogenizing the tissue specimens in the RIPA lysis buffer (25 mM Tris-HCl pH 7.6, 150 mM NaCl, 1% NP-40, 1% sodium deoxycholate, 0.1% SDS), and the concentration was determined by the Bradford protein assay (Bio-Rad, Hercules, CA). Equal amount of protein (50 mg/lane) was separated in 10% SDS-polyacrylamide gels and transferred to polyvinylidene fluoride membranes. For immunoblotting, membranes were blocked in 5% bovine serum for 1 h and incubated with primary antibody overnight at 4°C (Table S3). Membranes were washed three time by Tris-buffered saline containing 0.1% Tween-20 (TBST) and incubated with peroxidase-conjugated secondary antibody for 1 h at room temperature. After three times wash by TBST, the signal was detected with chemiluminescent substrates. Densitometric analysis was performed using Quantity One software to quantify the optical densities (OD value) of each protein band. GAPDH was used as the internal control.

2.5 | In situ hybridization

ISH was performed using commercially available kits (Boster, Wuhan, China). High-performance liquid chromatography (HPLC)-purified oligonucleotide probes specific for VEGF-C (Cat: K2145), VEGFR-2 (Cat: MK1438) and VEGFR-3 (Cat: MK1439) mRNA were used following manufacturer's protocol. Paraffin sections were cut at 6 μm thicknesses, dewaxed, hydrated, and immersed in 3% H_2O_2 for 10 min sequentially at room temperature. After treated with pepsin (100 μg/ml in 3% citric acid) at 37°C for 30 min and pre-hybridization solution (50% deionized formamide, 0.5 mg/ml heparin, 0.5 mg/ml Torula RNA, 0.1% Tween 20, 5X SCC and

9.2 mM citric acid) at 38°C for 3 h, sections were hybridized with DIG-UTP-labeled oligonucleotide probe overnight at 38°C in a humidified chamber with 20% glycerin. After rinse, sections were further treated with confining liquid at 37°C for 30 min, and stained with a SABC peroxidase system (AR0148, Boster, Wuhan, China) with 3,3′-diaminobenzidine (DAB) as the chromogen, and counterstained with hematoxylin. Finally, sections were dehydrated and sealed with Cytoseal 60 (Thermo Scientific, Wilmington, USA). Phosphate-buffered saline (PBS) with nonsense probe without probe was used as the negative control for the hybridization. An inverted bright-field microscope (DMIRB, LEICA, Nussloch, Germany) was used to acquire images.

2.6 | Immunohistochemistry

Paraffin embedded samples were sectioned at 6 μm thickness and spread on polylysine-coated slides. Sections were deparaffinized, rehydrated, and treated with 0.3% H_2O_2 to remove endogenous peroxidase activity. For antigen retrieval, sections were microwaved in citrate buffer (0.01 M, pH 6.0) for 20 min at 98°C. After washing with PBS, sections were blocked by 10% normal goat serum for 45 min and incubated with the primary antibody overnight at 4°C. Sections were then washed and incubated with horseradish peroxidase-conjugated secondary antibody for 1 h at 37°C after. Finally, the signal was developed by DAB. Counterstaining was performed with hematoxylin. To ensure the specificity of the IHC signals, negative control experiments were performing in parallel, using secondary antibody alone. Images were acquired similarly with ISH.

2.7 | Immunofluorescence

Sections at 10 μm thickness were cut from dehydrated tissues using a cryostat microtome (Cm3000, Leica, Nussloch, Germany). After three times wash in PBS, sections were blocked in 10% normal goat serum and incubated with the primary antibody overnight at 4°C. Sections were then washed and incubated accordingly with Alexa Fluor 488-conjugated anti-rabbit antibody (Thermo Fisher Scientific Cat# A-11008, RRID:AB_143165) or Alexa Fluor 555-conjugated anti-mouse antibody (Thermo Fisher Scientific Cat# A-21422, RRID:AB_2535844). Sections were subsequentially nuclear stained by Hoechst 33258, mounted, and photographed by a confocal microscope (TCS-TIV; Leica, Nussloch, Germany).

2.8 | Evaluation of ISH and IHC

For each section evaluated under the LEICA bright-field microscope, non-overlapping fields (200× magnification, 0.0625 mm × 0.0625 mm width) were defined in the center of the lesions as guiled by a square grid inserted into the eyepiece. DNs and BCs can be clearly distinguished from other cell components based on cytological properties. Following an evaluation scheme reported previously [16], the staining intensity was semi-quantified to a 4-point scale: 0: absent, 1: weak, 2: moderate, and 3: strong staining. All the areas of the slices were evaluated, and the score represents the predominant cell staining intensity in each section [24]. In addition, we semi-quantified the relative number of positive cells within FCD lesions according to a three-point frequency score: 1: 0%–10% (rare); 2: 11%–50% (sparse); 3: >50% (high). The product of these two scores (intensity and frequency) yielded the total score.

2.9 | Electrophysiological recording

Transverse slices (300 μm) of the medial parietal cortex of 3–4 weeks old FCD rats were obtained via a Leica vibratome (Leica, VT1000S) in cold sucrose-based solution (in mM): sucrose (300), KCl (2), NaH_2PO4 (1.25), $CaCl_2$ (1), $MgCl_2$ (5), $NaHCO_3$ (26), and glucose (11) and transferred to an oxygenated recovery chamber containing standard artificial cerebrospinal fluid (ACSF) (in mM): NaCl (140), KCl (2.5), NaH_2PO4 (1.4), $CaCl_2$ (2), $MgCl_2$ (2), $NaHCO_3$ (25), and glucose (11).

For action potential (AP) recording, the membrane was first clamped at −70 mV and applied with a series of stimulation range from −200 to +200 pA (stepped at 10 pA) or a constant tonic depolarizing stimulation at 200 pA after transferred to current clamp mode. The evoked EPSCs (eEPSCs) mediated by NMDA and AMPA (α-amino-3-hydroxy-5-methyl-4-isoxazole-propionicacid acid) receptors in dysmorphic neurons were stimulated through a glass micropipette (tip diameter 10–50 μm) and recorded by a lateral pipette (50–100 μm) [25]. AMPA receptor-mediated current was recorded at −70 mV and the negative peak upon stimulation was considered as the amplitude of AMPA current. NMDA current was recorded at +50 mV in the same neuron and considered as the positive peak at 80 ms upon stimulation. Picrotoxin (100 μM) was applied to block $GABA_A$ receptor-mediated inhibitory synaptic currents. For recording of puffed NMDA induced current, Mg^{2+} was omitted from the extracellular solution. For all the recording, ACSF was used as the external solution, and the pipette solution contained (in mM): 140 KCl, 0.5 EGTA, 5 MgATP, and 5 HEPES, pH 7.3 with KOH, and osmolality was 280–290 mΩ. VEGF-C and ki8751 were applied via the perfusion system.

The extracellular electrical stimulation was programmed with a stimulator (master-8-cp, A.M.P.I) and an isolator (iso-flex, A.M.P.I). The stimulating

current was set as 40–90 μA and 100–200 μs and repeated every 30 s. All the recordings were performed at room temperature with a HEKA EPC-10 amplifier. Signals were low-pass filtered at 2 kHz and digitized at 10 kHz. Cells were excluded from analysis if the series resistance increased by >15% during recording or exceeded 20 MΩ. Data were analyzed offline (clampfit 10, Mini analysis) and plotted in Origin 8 graphing software.

2.10 | Statistical analysis

The proper sample size and study power were estimated according to the previously established experimental settings [26]. Data acquisition and analysis were done blindly and were represented as mean ± SEM. For comparisons between two groups, unpaired two-tailed *t*-test was used. Statistical methods and number of replicates were indicated when used. Normality and equal variance tests were performed for all statistical analyses. Data were plotted and analyzed with Graphpad Prism 5, Origin 8 or SPSS 13 software. A $p < 0.05$ was considered as statistically significant.

3 | RESULTS

3.1 | The expressional profiles of VEGF-C, VEGFR-2, 3 in lesions of patients with focal cortical dysplasia

3.1.1 | The expression of VEGF-C, VEGFR-2, 3 was increased in the disorganized cortex of patients with focal cortical dysplasia

We first investigated the expressional difference of *VEGF-C*, *VEGFR-2*, and *VEGFR-3* between FCD lesions and control cortex (CTX) of patients. RT-PCR results showed that the mRNA expression of all three genes was increased in the FCD lesions, regardless of FCD subtypes (Figure 1A) (*$p < 0.05$, **$p < 0.01$, unpaired two-tailed *t*-test). Western blot detected the band of expected size, and quantification results showed that the protein expression of *VEGFR-2* was increased in all FCD subtypes, while *VEGF-C* and *VEGFR-3* was increased only in FCD IIa and FCD IIb lesions (Figure 1B) ($^{\#}p > 0.05$,*$p < 0.05$, **$p < 0.01$, unpaired two-tailed *t*-test).

Next, we perform ISH to investigate the cell type–specific mRNA expression of these genes. Consistent with our previous study [15], for *VEGF-C* mRNA expression, weak signal was observed in the pyramidal neurons and vascular endothelial cells in CTX (Figure 2A). In comparison, moderate signal was detected in the neurons lined in microcolumns and the vascular endothelial cells in FCD I lesion (Figure 2B, insert), and strong signal was detected in the DNs and BCs for FCD IIa and FCD IIb samples, respectively (Figure 2C,D). Similarly for *VEGFR-2* and *VEGFR-3*, weak ISH signal was detected in the pyramidal neurons of CTX, whereas the intensity were increased in the micro-columnar neurons, DNs and BCs in FCD I, FCD IIa, and FCD IIb lesions, relatively (Figure 2E–L). Together, we identified increased protein and mRNA expression of these *VEGF* genes in FCD lesions, with expression enriched in expected type of neurons and endothelial cells.

3.1.2 | Cell type–specific protein expression of VEGF-C in FCD lesions

Next, immunohistochemistry (IHC) and double immunofluorescence (IF) were performed to determine the cell type-specific protein expression of VEGF-C in CTX and FCD lesions. As shown in Figure 3A–C, the protein abundance of VEGF-C was enriched in the neurons of microcolumns in type I FCD sections. Double IF further revealed that these neurons were also NeuN positive, indicating that they belong to mature neurons (Figure 3D). VEGF-C was rarely expressed in the astrocytes of FCD I lesions, as indicated by infrequent co-staining with GFAP, a marker of astrocytes (Figure 3E). In FCD IIa samples, VEGF-C was intensely expressed in DNs and vascular endothelial cells (Figure 3F–H). Double IF identified strong VEGF-C immunoactivity in NeuN negative DNs (Figure 3I) and some GFAP positive astrocytes (Figure 3J). Notably, we did not detect GFAP signal in any DNs from the FCD IIa samples. In FCD IIb sections, VEGF-C signal was identified in BCs by IHC (Figure 3K). VEGF-C signal was detected in DNs, but not in NeuN positive neurons (Figure 3L). However, VEGF-C was identified in NF-200 positive DNs (Figure 3M) and vimentin (a maker of immature neurons) [27] positive BCs (Figure 3N), suggesting that differentiating characteristic was altered in the DNs and BCs of FCD IIb lesions. In addition, VEGF-C immunoactivity was detected in a few GFAP positive astrocytes and CD68 positive microglial cells (macrophage-like morphology) in dysplastic cortex of FCD IIb lesions (Figure 3O,P).

3.1.3 | Cell type–specific protein expression of VEGFR-2 in focal cortical dysplasia lesions

Consistent with what previously reported [28], VEGFR-2 immunoactivity was detected in the pyramidal neurons and vascular endothelial cells in CTX (Figure 4A). Intensified VEGFR-2 immunostaining

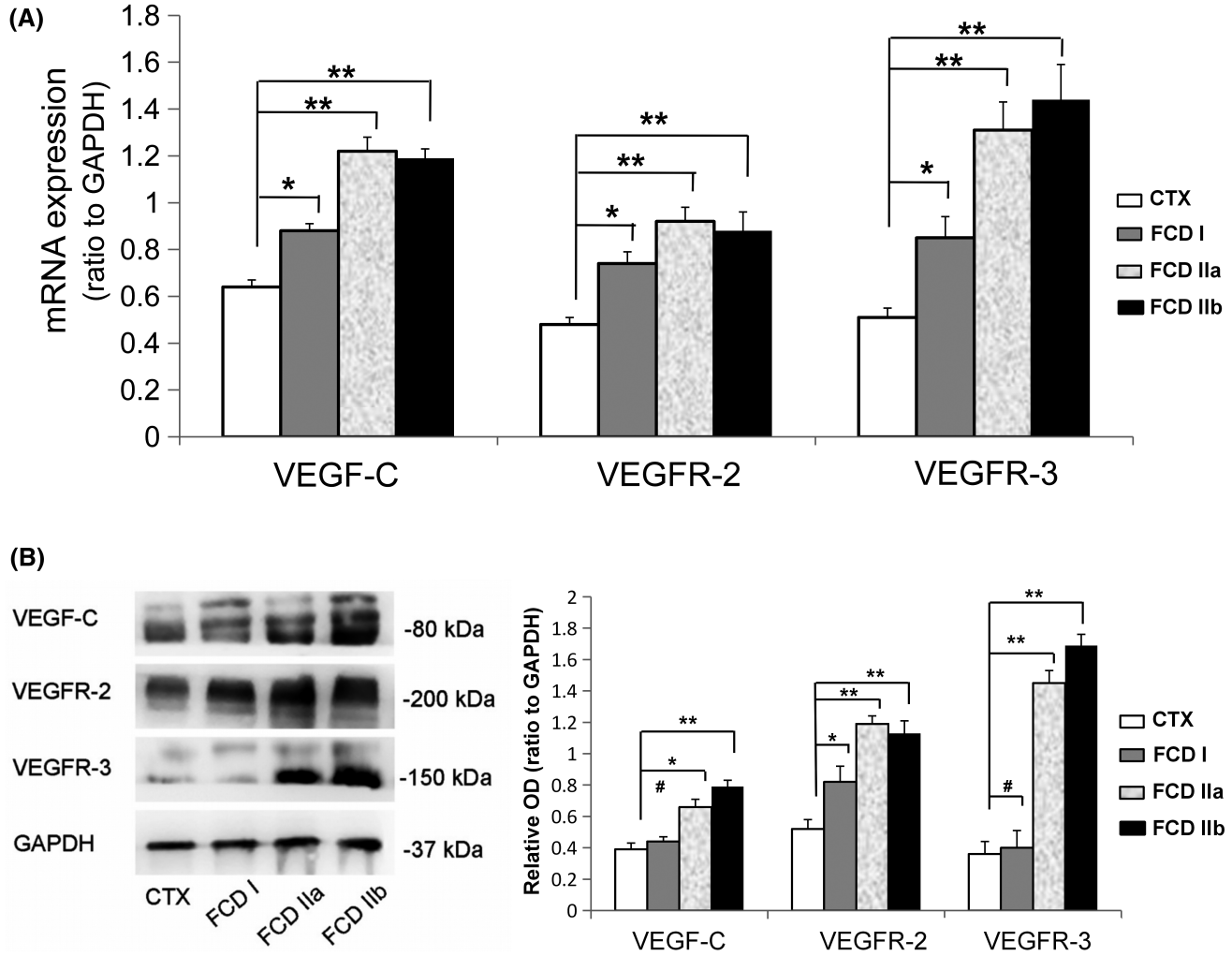

FIGURE 1 The mRNA and protein expression of VEGF-C and VEGFR-2, 3 were increased in the cortical lesions of patients with focal cortical dysplasia (FCD I), FCD IIa, and FCD IIb. (A) Statistical analyses indicated the mRNA of *VEGF-C*, *VEGFR-2*, and *VEGFR-3* was increased in FCD I, FCD IIa, and FCD IIb lesions compared with CTX. $*p < 0.05$, $**p < 0.01$, unpaired two-tailed *t*-test. $n = 10$, 11, 10 and 12 specimens in each group. (B) Representative immunoblot bands of VEGF-C (~80 kDa), VEGFR-2 (~200 kDa), VEGFR-3 (~150 kDa), and GAPDH (~37 kDa, loading control) in total homogenates from CTX and FCD lesions. Densitometric analyses showed that the expression of VEGF-C and VEGFR-3 was increased in FCD IIa and FCD IIb lesions, and the expression of VEGFR-2 was increased in FCD I, FCD IIa, and FCD IIb lesions. $^{\#}p > 0.05$, $*p < 0.05$, $**p < 0.01$, unpaired two-tailed *t*-test. $n = 10$, 12, 12, and 12 specimens in each group

was observed in the micro-columnar neurons of FCD I samples (Figure 4B). Double IF verified that VEGFR-2 was expressed in NeuN positive micro-columnar neurons and GFAP positive astrocytes (Figure 4C,D). IHC revealed strong VEGFR-2 immunoactivity in DNs of FCD IIa sections (Figure 4E), and Double IF further identified VEGFR-2 signal in NF-200 positive neurons (Figure 4F), GFAP positive astrocytes (Figure 4G,H), and NeuN positive neurons (Figure 4I). GFAP immunoactivity was not detected in VEGFR-2 positive DNs (Figure 4J). In FCD IIb cases, VEGFR-2 was intensely expressed in DNs and BCs and weakly expressed in vascular endothelial cells (Figure 4K). Double IF showed that VEGFR-2 was expressed in NF-200 positive neurons but not NeuN positive neurons (Figure 4L,M). VEGFR-2 was also expressed in vimentin positive BCs and GFAP positive astrocytes (Figure 4N–P). GFAP activity was not detected in VEGFR-2 positive DNs (Figure 4Q).

3.1.4 | Cell type–specific protein expression of VEGFR-3 in focal cortical dysplasia lesions

VEGFR-3 IHC detected weak signal in the pyramidal neurons and vascular endothelial cells in CTX (Figure 5A). In FCD I lesion, VEGFR-3 immunoreactivity was detected in the micro-columnar neurons (Figure 5B). Double IF further revealed that VEGFR-3 was expressed in NeuN positive neurons and some GFAP positive astrocytes (Figure 5C,D). In sections

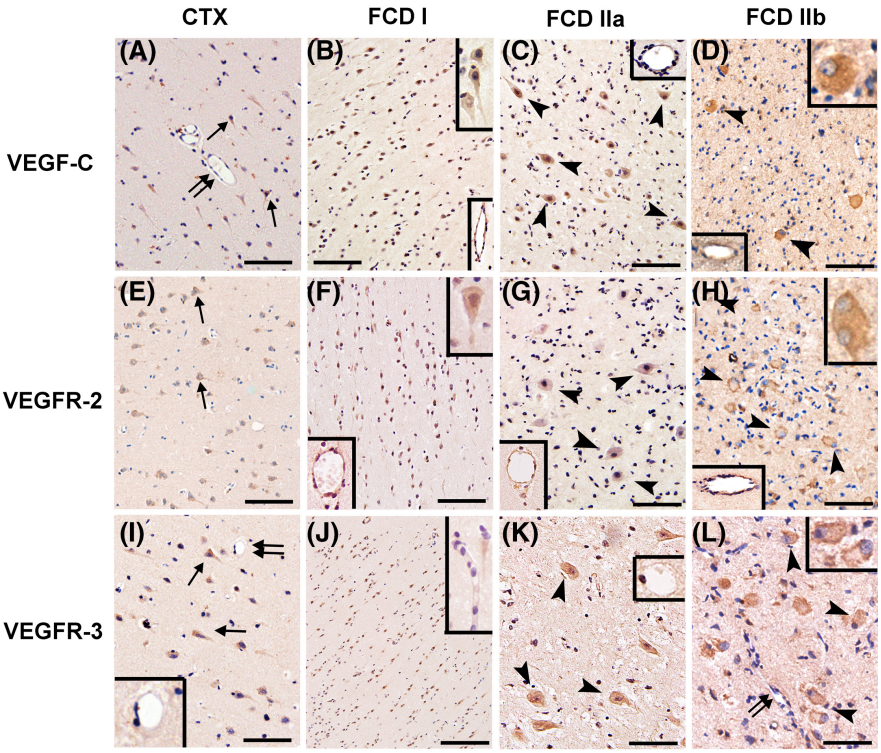

FIGURE 2 In situ hybridization showed the mRNA expression of *VEGF-C*, *VEGFR-2*, and *VEGFR-3* in micro-columnar neurons, dysplastic neurons (DNs) and balloon cells (BCs) in focal cortical dysplasia (FCD) lesions. (A) Weak *VEGF-C* mRNA was observed in the pyramidal neurons (arrows) and endothelial cells of blood vessels (double arrows) in CTX. (B) Moderate *VEGF-C* mRNA was observed in the micro-columnar neurons (upright inset) and vascular endothelial cells (downright inset) in FCD I lesion. (C and D) Strong *VEGF-C* mRNA signal was detected in DNs (arrowheads in c) and BCs (arrowheads and upright inset in d) in FCD type II lesion and relatively moderate *VEGF-C* mRNA was detected in the vascular endothelial cells in FCD IIa (upright inset in C) and IIb lesions (bottom left inset in D). (E) Weak *VEGFR-2* mRNA was identified in the pyramidal neurons of CTX (arrows). (F) Moderate to strong *VEGFR-2* mRNA signal was detected in micro-columnar neurons (upright inset) and vascular endothelial cells (bottom left inset) in FCD I lesion. (G and H) Strong *VEGFR-2* mRNA was detected in DNs (arrowheads in G) and BCs (arrowheads and upright inset in H) in type II FCD lesions; moderate *VEGFR-2* mRNA signal was detected in the vascular endothelial cells in FCD IIa lesions (bottom left insets). (I) Weak *VEGFR-3* mRNA (arrows) expression was detected in the pyramidal neurons in CTX, but barely in blood vessels (double arrows and inset). (J) Moderate *VEGFR-3* mRNA was detected in the micro-columnar neurons (inset) in FCD I lesion. (K and L) Strong *VEGFR-3* mRNA signal was detected in DNs (arrowheads in K) and BCs (arrowheads and inset in L) in FCD type II lesions, but barely in vascular endothelial cells (inset in K and double arrows in L). Scale bars: 100 μm in A–L; 20 μm in insets

of FCD IIa lesions, VEGFR-3 was intensely expressed in DNs (Figure 5E). Double IF results showed that VEGFR-3 was expressed in NF-200 positive neurons but not in NeuN positive neurons (Figure 5F–I). Weak VEGFR-3 signal was detected in a few GFAP positive astrocytes (Figure 5J,K). In FCD IIb lesions, strong immunoactivity of VEGFR-3 was observed in DNs and BCs but barely in the vascular endothelial cells (Figure 5L). Double IF results indicated that VEGFR-3 was abundantly expressed in NF 200 positive neurons but not in NeuN positive neurons (Figure 5M–O). Additionally, we did not detect co-expression of VEGFR-3 and vimentin in BCs (Figure 5P). VEGFR-3 was not detected in GFAP positive astrocytes either (Figure 5Q).

We evaluated the immunoreactivity score of VEGF-C, VEGFR-2, and VEGFR-3 in CTX and three types of FCD lesions by semi-quantitative analysis, as shown in Figure S1 and Table S4.

3.2 | The modulatory effects of VEGF-C on dysmorphic neurons in rats with focal cortical dysplasia

3.2.1 | Electrophysiological characteristics of neurons in experimental rats with focal cortical dysplasia

Next, we used in utero X-ray radiated rats to mimic the pathological characteristics of patients with FCD [22, 23]. X-ray-radiated rats showed dramatically deformed and reduced telencephalon and cerebellum at 30 days after birth, and HE staining further revealed that the hierarchy of cortical layers was abnormally disturbed (Figure 6A). The morphology of dysmorphic neurons was distinctive from normal pyramidal neurons under infrared differential interference contrast (IR-DIC) microscope, as characterized by cortical loss of polarity in morphology (Figure 6B). Subsequently, we investigated

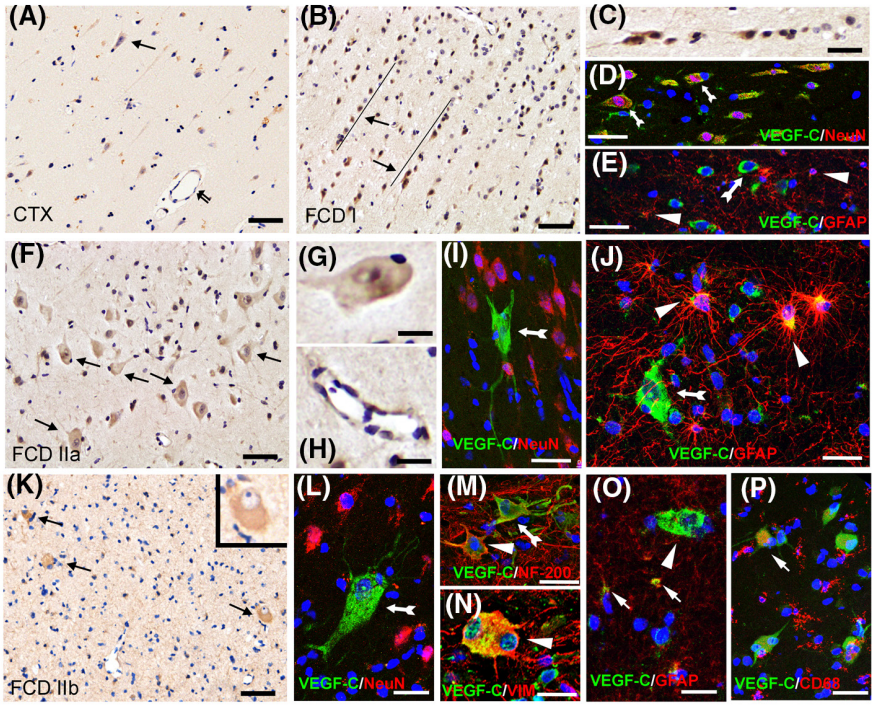

FIGURE 3 Cell type–specific expression of VEGF-C in cortical lesions of patients with focal cortical dysplasia (FCD). (A) Immunohistochemitry (IHC) results revealed weak VEGF-C staining in the pyramidal neurons (arrows) and vascular endothelial cells (double arrows) in CTX. (B, C) Strong VEGF-C immunoreactivity was detected in the micro-columnar neurons in FCD I lesion. (D) VEGF-C was expressed in NeuN positive neurons (arrows). (E) VEGF-C was expressed in neurons (arrows) but not in GFAP positive astrocytes (arrowheads). (F–H) Moderate to strong VEGF-C immunoreactivity was detected in dysplastic neurons (DNs) (arrows) and vascular endothelial cells in FCD IIa lesions. (I) Double IF showed that VEGF-C (arrows) was not expressed in NeuN positive neurons. (J) VEGF-C was expressed in DNs (arrows), and a few GFAP positive astrocytes (arrow heads). (K) Strong VEGF-C immunoreactivity was detected in balloon cells (BCs) (arrows and insets) in FCD IIb lesion. (L) Strong VEGF-C immunoreactivity was detected in NeuN absent DNs (arrows) in FCD IIb lesion. (M) VEGF-C was expressed in NF-200 positive neurons (arrow), and neurons with weak NF-200 signal (arrowhead). (N) VEGF-C was expressed in vimentin (VIM, arrow) positive BCs. (O) Strong VEGF-C immunoreactivity was detected in BCs (arrowhead) and a few GFAP positive astrocytes (arrows). (P) VEGF-C immunoreactivity was detected in a few CD68 positive microglial cells in FCD IIb lesion (arrow). Scale bars: 60 μm for A; 100 μm for B; 50 μm for C–F; 20 μm for G; 30 μm for H–P

the electrophysiological properties of dysmorphic neurons in the medial parietal cortex of this FCD rat model. As the representative traces and statistical analysis showed, the threshold of AP firing induced by stepped current was similar in control and dysmorphic neurons (Figure 6C,D) ($^{\#}p > 0.05$, unpaired two-tailed *t*-test). However, the ability of spike frequency adaption [29, 30], which represents the ability of reduplicative discharges of AP to a sustained injection of depolarizing rectangular currents was significantly attenuated in dysmorphic neurons under tonic stimulation (200 pA, 1000 ms) (Figure 6E). This observation suggests that the electrophysiological function is impaired in dysmorphic neurons.

Next, we investigated the amplitude of evoked-EPSC (eEPSC) in dysmorphic neurons. As the representative traces and statistical analyses showed (Figure 6F–H), the amplitude and the current area (amplitude × time) of eEPSC were both increased in the dysmorphic neurons ($^{*}p < 0.05$, unpaired two-tailed *t*-test), suggesting the efficiency of synaptic transmission was enhanced in the disorganized cortex. As NMDA receptor on postsynaptic membrane determines the amplitude of eEPSC, we examined the ratio of NMDA receptor- and AMPA receptor-mediated eEPSCs (the NMDA/AMPA ratio of eEPSC) in dysmorphic neurons. As the representative traces and statistical analyses showed (Figure 6I,J), the NMDA/AMPA ratio of eEPSC was increased in dysmorphic neurons ($^{*}p < 0.05$, unpaired two-tailed *t*-test), suggesting that the function of NMDA receptor was upregulated in the dysmorphic neurons of FCD rats.

3.2.2 | VEGF-C potentiated NMDA receptor-mediated current in dysmorphic neurons

Finally, we investigated the relationship between the expression of VEGF-C system and NMDA receptor-mediated current using the FCD rat model. Using similar IF approach described above, weak VEGF-C, VEGFR-2, and negligible VEGFR-3 immunoreactivity was detected in the cortical neurons of control rats, while the signal for all the three proteins was increased in the cortical neurons of FCD rats (Figure7A).

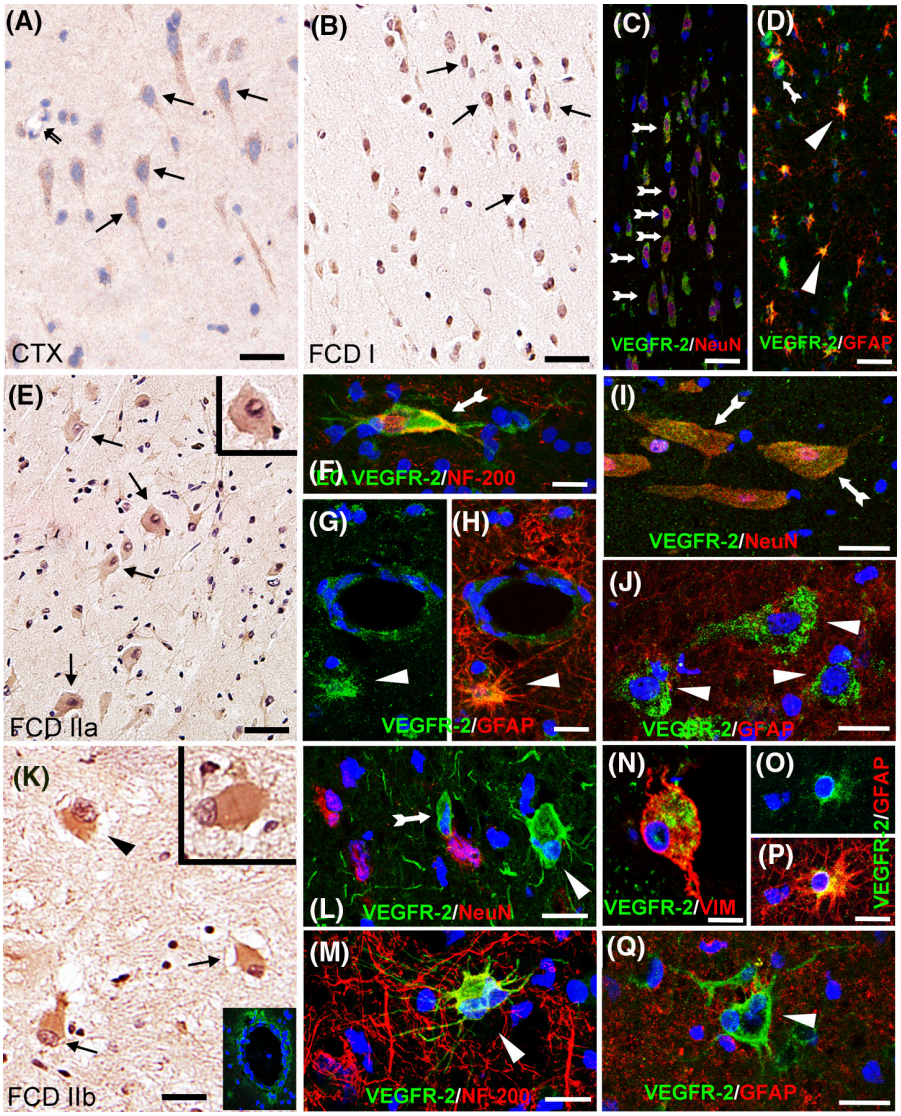

FIGURE 4 Cell type-specific expression of VEGFR-2 in focal cortical dysplasia lesions. (A) Immunohistochemistry results revealed weak VEGFR-2 immunoreactivity in the pyramidal neurons (arrows) and vascular endothelial cells (double arrows) in CTX. (B) Moderate VEGFR-2 immunoreactivity was detected in micro-columnar neurons (arrows) in FCD I lesions. (C and D) VEGFR-2 was expressed in NeuN positive micro-columnar neurons (arrows) and GFAP positive astrocytes (arrowheads) in FCD I lesions. (E) Moderate to strong VEGFR-2 immunoreactivity was detected in dysplastic neurons (DNs) (arrows and inset) in FCD IIa lesions. (F–I) VEGFR-2 was expressed in NF-200 positive neurons (arrows), GFAP positive astrocytes (arrowheads) and NeuN positive neurons (arrows) in FCD IIa lesions. (J) GFAP signal was not detected in VEGFR-2 expressed DNs in FCD IIa lesions. (K) Strong VEGFR-2 immunoreactivity was detected in DNs (arrows), balloon cells BCs (arrowhead and top right inset) and vascular endothelial cells (bottom right inset) in FCD IIb lesions. (L) VEGFR-2 immunoreactivity was detected in NeuN negative DNs (arrow) and BCs (arrowhead) in FCD IIb lesions. (M) VEGFR-2 was expressed in NF-200 positive neurons (arrowhead). (N–P) VEGFR-2 was expressed in vimentin (VIM) positive BCs, and GFAP positive astrocytes. (Q) GFAP signal was not detected in VEGFR-2 positive BCs in FCD IIb lesion. Scale bars: 60 μm for A; 100 μm for B; 50 μm for C-F, I-K; 30 μm for H-M; 20 μm for G, H, N–P

VEGF-C system exhibited neuroprotective effect in a range of neurological diseases [12, 13, 31], and therefore we wondered whether the upregulated expression of VEGF-C system could modulate the function of NMDA receptors in the dysmorphic neurons. In the recorded neurons, NMDA induced an excitatory current, whose amplitude was increased upon the continuous VEGF-C perfusion and reduced after the washout of VEGF-C for 20 min (Figure 7B,C) (*$p < 0.05$, unpaired two-tailed *t*-test). Because our previous staining results suggest that VEGFR-2 is likely to be one of the predominant VEGF-C receptors in the dysmorphic neurons in FCD lesions, we next tried to perturb VEGF signaling pathway by applying ki8751, a specific inhibitor for VEGFR-2. As shown in Figure 7D,E, NMDA induced a depolarizing current in the recorded cell upon ki8751 treatment. Importantly, the boosting effect of VEGF-C on NMDA-induced current was inhibited in the presence of ki8751, and washout of VEGF-C thereafter did not alter the amplitude of NMDA current. These observations indicated that the effect of VEGF-C on the amplitude of NMDA receptor-mediated current was dependent on binding

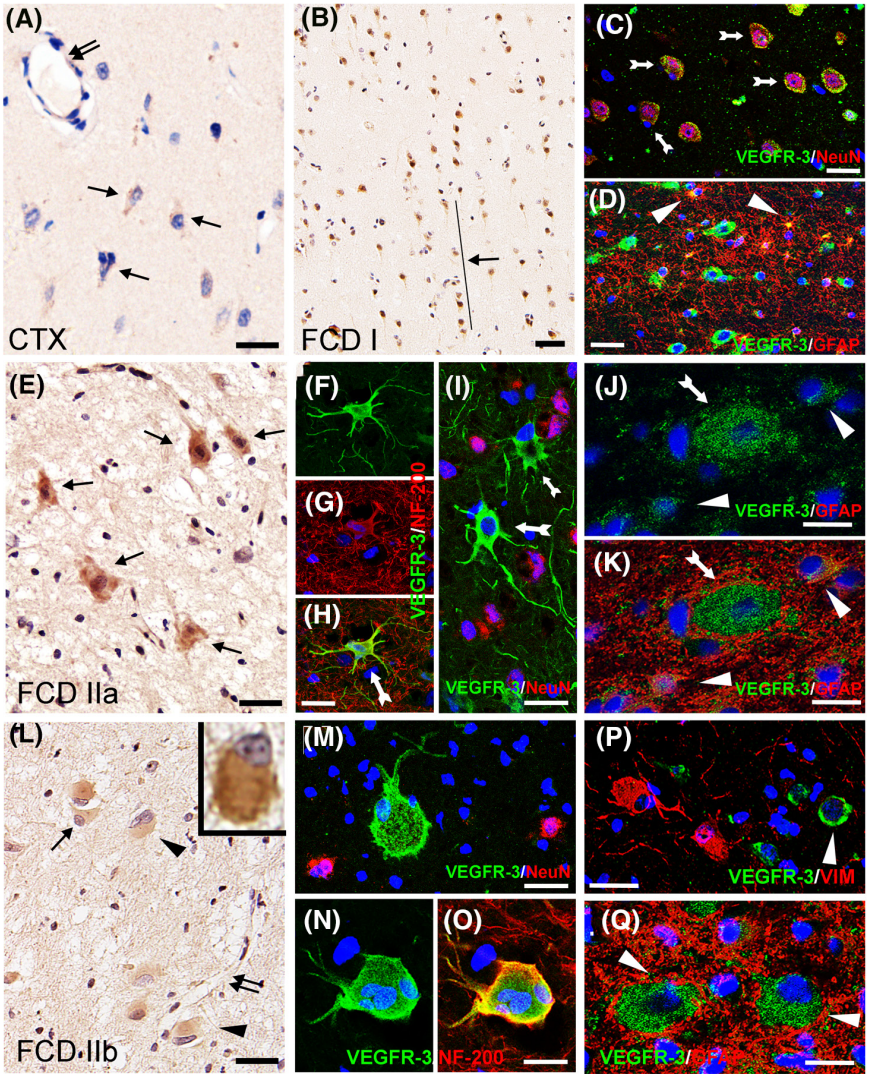

FIGURE 5 Cell type-specific expression of VEGFR-3 in FCD lesions. (A) VEGFR-3 immunoreactivity was not detected or very weak in the neurons (arrows) or vascular endothelial cells (double arrows) in CTX. (B) Weak VEGFR-3 immunoreactivity was detected in the micro-columnar neurons (arrow) in FCD I lesion. (C and D) VEGFR-3 was expressed in NeuN positive micro-columnar neurons (arrows) and few GFAP positive astrocytes (arrowheads) in FCD I lesion. (E) Strong VEGFR-3 immunoreactivity was detected in DNs (arrows) in FCD IIa lesion. (F–H) VEGFR-3 was expressed in NF-200 positive neurons (arrow). (I) VEGFR-3 was not expressed in NeuN positive neurons (arrows) in FCD IIa lesion. (J and K) VEGFR-3 was expressed in GFAP negative DNs (arrow), and a few GFAP positive astrocytes (arrowheads) in FCD IIa lesion. (L) Moderate to strong VEGFR-3 immunoreactivity was detected in DNs (arrow) and BCs (arrowheads and inset) in FCD IIb lesion, and barely in vascular endothelial cells (double arrows). (M–O) VEGFR-3 immunoreactivity was detected in NF-200 positive neurons but not in NeuN positive neurons. (P) VEGFR-3 signal was not detected in vimentin positive BCs (arrowhead). (Q) VEGFR-3 signal was detected in BCs (arrowheads), but not in GFAP positive astrocytes in FCD IIb lesion. Scale bars: 60 μm for A; 100 μm for B; 50 μm for C–I, L, P; 30 μm for H–M; 20 μm for J, K, M–O, Q

to VEGFR-2. Together, our results suggested that in FCD lesion, increased expression of VEGF-C system might partially account for the abnormality of NMDA receptor-mediated current.

4 | DISCUSSION

Here, we characterized the cell type–specific expression of VEGF-C and its receptors, VEGFR-2 and VEGFR-3 at both mRNA and protein levels in the cortical lesions resected from intractable epilepsy patients with FCD. The comparison between FCD lesion and CTX tissues further identified increased gene expression of the VEGF-C system under the disease context. By using the FCD rat model, we provided evidence suggesting that elevated VEGF signaling might be linked to the abnormal NMDA receptor-mediated current in FCD.

Previous studies found that VEGF-C system plays neurotrophic roles in neural development [11, 12, 32] and neurological diseases, such as ischemia [13, 33–35,], brain tumor [36–38], and Alzheimer's disease [39]. In patients with epilepsy and animal models, VEGF-C and its receptors were found to be upregulated in the epileptogenic

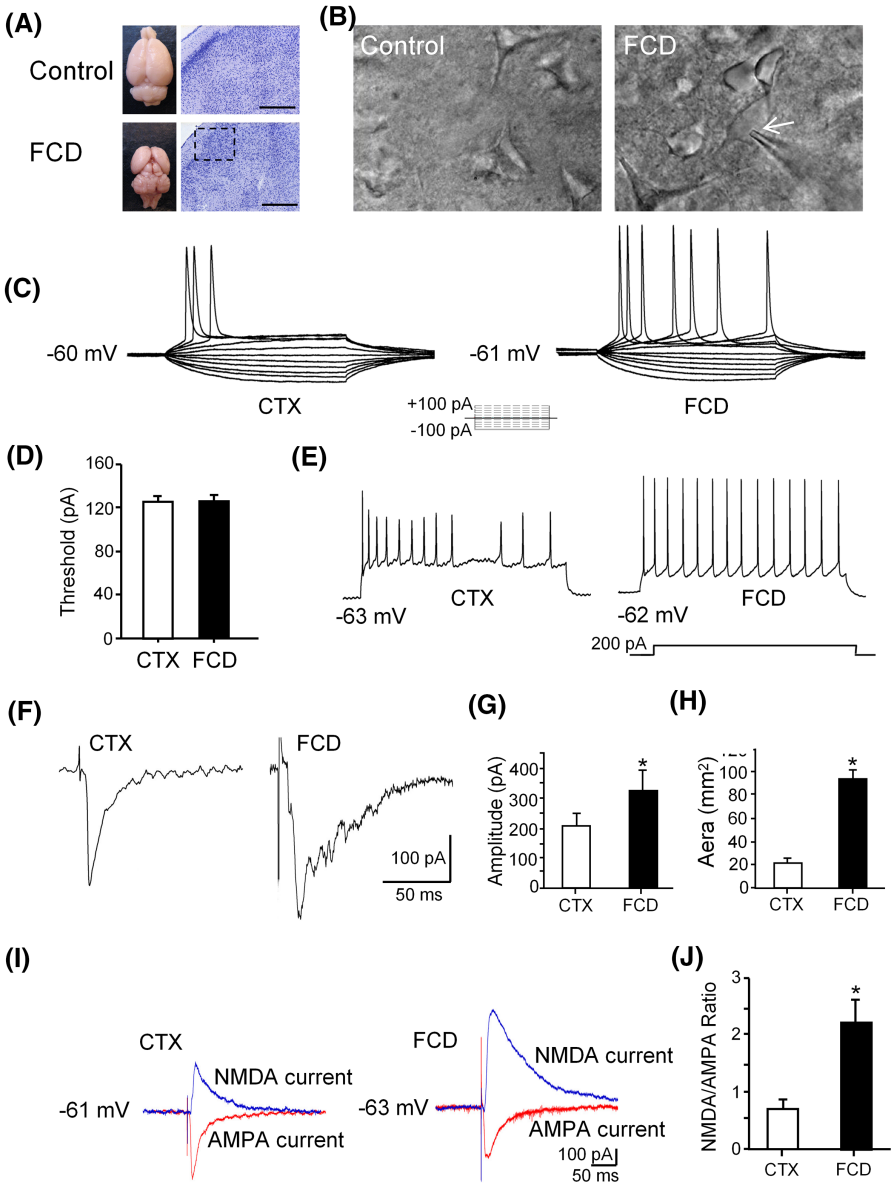

FIGURE 6 The excitability of dysmorphic neurons in the dysplastic cortex of FCD rats was altered. (A) Representative brain images from control and X-ray irradiated rats (FCD). Note the reduced volume of telencephalon, exposed quadrigemina and increased cerebellum in the FCD brain. Representative images of HE staining showing the hierarchy of cortex was disrupted in FCD rat. Scale bars: 100 μm. (B) Dysmorphic neurons lost polarity under observation with IR-DIC microscope during electrophysiological recording. Arrow indicated the recording malformed neuron. (C and D) Representative traces of action potential firing in control and dysmorphic neurons under stepped current stimulation. Statistical analysis revealed that the threshold of action firing was similar between control and dysmorphic neurons. $p > 0.05$, unpaired two-tailed t-test. $n = 93$, 118 neurons from 15, 19 rats in each group, respectively. (E) Representative traces showing the ability of accommodation to tonic depolarizing stimulation was impaired in dysmorphic neurons. (F–H) The amplitude and the area of eEPSC were increased in the dysmorphic neurons. *$p < 0.05$, unpaired two-tailed t-test. $n = 19$, 22 neurons from five, six rats in each group. (I and J) The NMDA/AMPA ratio of eEPSC was increased in the dysmorphic neurons in FCD rats. *$p < 0.05$, unpaired two-tailed t-test. $n = 15$ or 22 neurons from five or six rats in each group

foci [15, 40]. Our previous study also identified increased expression of VEGF-C system in the cortical tubers of intractable epilepsy patients with tuberous sclerosis complex (TSC) [16]. Here, we found that VEGF-C, VEGFR-2 and VEGFR-3 were weakly expressed in the CTX from control subjects, in line with the expression pattern of VEGF-C system reported in adults previously [12]. In comparison, their expression was increased in the cortical lesions of patients with FCD, especially in the dysmorphic cells. Interestingly, NeuN was found to be absent from VEGF-C positive DNs and BCs, suggesting the immature characteristic of dysmorphic neurons in FCD lesions [27].

We used prenatal X-ray irradiation induced FCD rat model to investigate the role of VEGF-C system in the regulation of the excitability of dysmorphic neurons

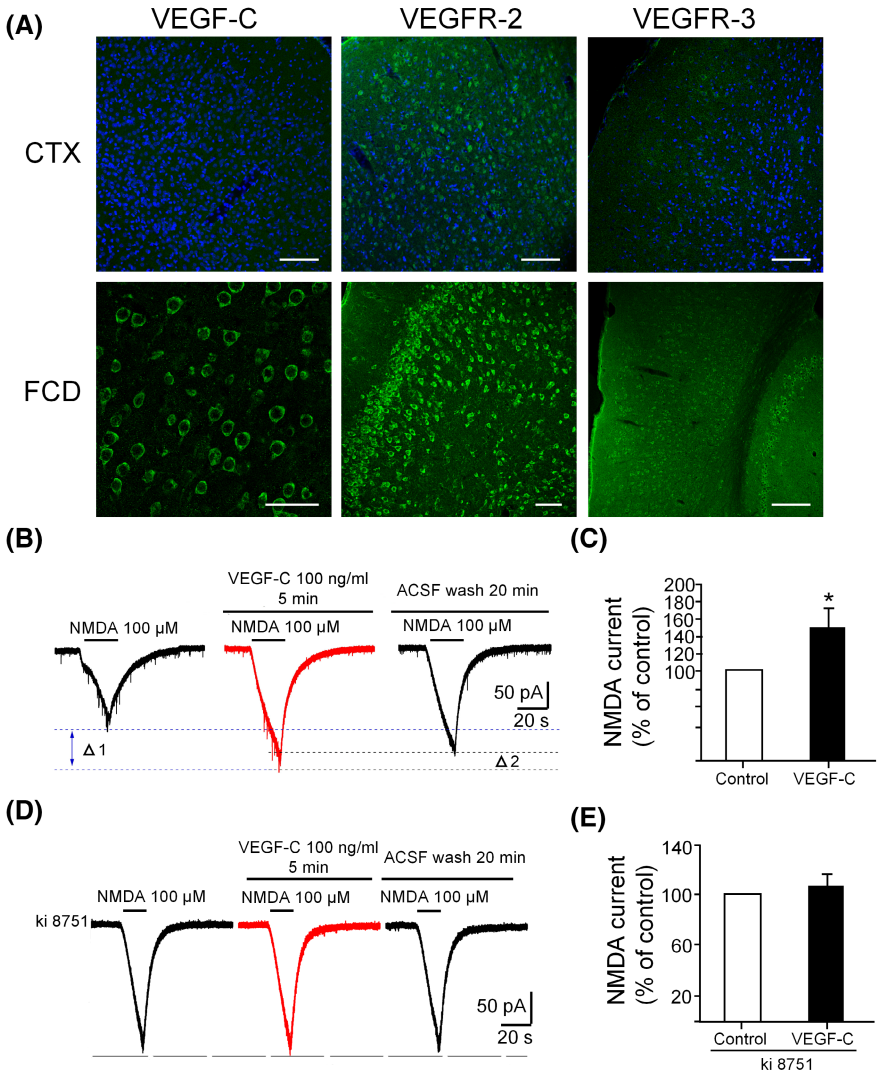

FIGURE 7 VEGF-C potentiated NMDA induced current in the dysmorphic neurons of FCD rats. (A) Immunostaining images showing the increased immunoreactivity of VEGF-C, VEGFR-2 and VEGFR-3 in the neurons in dysplastic cortex. Scale bar: 100 μm. (B and C) Representative traces and statistical analyses showing that VEGF-C increased the amplitude of NMDA-induced current in the dysmorphic neurons and washout of VEGF-C abolished the increasement. *$p < 0.05$, unpaired two-tailed t-test. $n = 14$ neurons from five rats. (D and E) The promoting effect of VEGF-C on NMDA-induced current was blocked in the existence of the specific VEGFR-2 inhibitor, ki8751. $p > 0.05$, unpaired two-tailed t-test. $n = 9$ neurons from three rats

[41, 42]. The dysmorphic neurons in the FCD rats displayed several functional aberrations, such as loss of polarity, increased NMDA receptor-mediated current and NMDA/AMPA ratio of eEPSCs. Although the NMDA receptor has been reported to be increasingly expressed in the cortical lesions of FCD patient [43–46], less is known related to its function in dysmorphic neurons. Our electrophysiological findings from the animal model suggest that the excitatory synaptic transmission was enhanced via NMDA receptor in dysmorphic neurons.

By using the animal model, our study helped to build the relationship between VEGF-C system and NMDA receptor-mediated current in FCD. In neurons isolated from the FCD rats, the amplitude of the excitatory current induced by NMDA was increased upon continuous VEGF-C perfusion and reduced after VEGF-C washout. Moreover, the enhancing effect of VEGF-C on NMDA-induced current were antagonized by the specific VEGFR-2 inhibitor, ki8751, indicating that VEGF-C and VEGFR-2 system regulates the function of NMDA receptors in dysmorphic neurons. Because the expression of VEGF-C and VEGFR-2 was increased in the cortical lesions of patients with FCD, we speculated that the upregulated VEGF-C system might contribute to the epileptogenicity in FCD patients by modulating NMDA receptors mediated excitatory transmission. Following this functional linkage, further mechanistic study might be carried out to understand how the VEGF signaling cascade regulates the NMDA receptors and other neuronal ion channels.

5 | CONCLUSIONS

Our study characterized the expression of VEGF-C, VEGFR-2, and VEGF-3 in FCD lesions and showed potential linkage between the VEGF-C system and the abnormal NMDA current during the pathogenesis of FCD. These results advanced our standing of the etiology of FCD and further suggested that targeting the VEGF-C system might be an important FCD treatment strategy.

ACKNOWLEDGMENTS

This work was supported by the grants from National Natural Science Foundation of China (No. 81771217, No. 81873757), Training project of clinical medical researcher of Army Medical University (No. 2018XLC3046), Chongqing Technology Innovation and Application Development Special key Project (cstc2019jscx-dxwtBX 0010) and Chongqing Scientific and health Joint medical scientific research project (No. 2019MSXM099).

CONFLICT OF INTEREST

The authors declare that they have no competing interests.

AUTHOR CONTRIBUTIONS

Kai-Feng Shen, Qing-Tian Duan, and Chun-Qing Zhang contributed to conception and study design; Kai-Feng Shen, Qing-Tian Duan, Wei Duan, Sen-Lin Xu, Yan-Yan Ke, and Li-Ting Wang contributed to acquisition and analysis of data, and Ning An, Shi-Yong Liu, Hui Yang, and Chun-Qing Zhang, contributed to surgery performance on the patients; Kai-Feng Shen, Qing-Tian Duan, and Chun-Qing Zhang contributed to verify the underlying data, interpretation of results and preparation of figures; Kai-Feng Shen, Qing-Tian Duan, and Chun-Qing Zhang, contributed to draft and revise the manuscript and figures. All authors edited and approved the paper.

DATA AVAILABILITY STATEMENT

Source data of this study are available upon reasonable request.

ORCID

Chun-Qing Zhang https://orcid.org/0000-0003-1171-436X

REFERENCES

1. Palmini A, Holthausen H. Focal malformations of cortical development: a most relevant etiology of epilepsy in children. Handb Clin Neurol. 2013;111:549–65.
2. Zhao YZC, Wang ZY, Cheng TY, Qin XY, Deng J, Fang X, et al. Vagal nerve stimulation is effective in pre-school children with intractable epilepsy: a report of two cases. J Neurorestoratology. 2020;8(3):149–59.
3. Mühlebner A, Gröppel G, Dressler A, Reiter-Fink E, Kasprian G, Prayer D, et al. Epilepsy surgery in children and adolescents with malformations of cortical development–outcome and impact of the new ILAE classification on focal cortical dysplasia. Epilepsy Res. 2014;108(9):1652–61.
4. Najm IM, Tilelli CQ, Oghlakian R. Pathophysiological mechanisms of focal cortical dysplasia: a critical review of human tissue studies and animal models. Epilepsia. 2007;48(Suppl 2):21–32.
5. Abdijadid S, Mathern GW, Levine MS, Cepeda C. Basic mechanisms of epileptogenesis in pediatric cortical dysplasia. CNS Neurosci Ther. 2015;21(2):92–103.
6. Cepeda C, Chen JY, Wu JY, Fisher RS, Vinters HV, Mathern GW, et al. Pacemaker GABA synaptic activity may contribute to network synchronization in pediatric cortical dysplasia. Neurobiol Dis. 2014;62:208–17.
7. Apte RS, Chen DS, Ferrara N. VEGF in signaling and disease: beyond discovery and development. Cell. 2019;176(6):1248–64.
8. Chen J-C, Chang Y-W, Hong C-C, Yu Y-H, Su J-L. The role of the VEGF-C/VEGFRs axis in tumor progression and therapy. Int J Mol Sci. 2012;14(1).
9. Liang X, Xu F, Li X, Ma C, Zhang Y, Xu W. VEGF signal system: the application of antiangiogenesis. Curr Med Chem. 2014;21(7):894–910.
10. Han J, Calvo C-F, Kang TH, Baker KL, Park J-H, Parras C, et al. Vascular endothelial growth factor receptor 3 controls neural stem cell activation in mice and humans. Cell Rep. 2015;10(7):1158–72.
11. Kwon H-B, Fukuhara S, Asakawa K, Ando K, Kashiwada T, Kawakami K, et al. The parallel growth of motoneuron axons with the dorsal aorta depends on Vegfc/Vegfr3 signaling in zebrafish. Development. 2013;140(19):4081–90.
12. Le Bras B, Barallobre M-J, Homman-Ludiye J, Ny A, Wyns S, Tammela T, et al. VEGF-C is a trophic factor for neural progenitors in the vertebrate embryonic brain. Nat Neurosci. 2006;9(3):340–8.
13. Shin Y-J, Choi J-S, Lee J-Y, Choi J-Y, Cha J-H, Chun M-H, et al. Differential regulation of vascular endothelial growth factor-C and its receptor in the rat hippocampus following transient forebrain ischemia. Acta Neuropathol. 2008;116(5):517–27.
14. Ward MC, Cunningham AM. Developmental expression of vascular endothelial growth factor receptor 3 and vascular endothelial growth factor C in forebrain. Neuroscience. 2015;303:544–57.
15. Sun F-J, Wei Y-J, Li S, Guo W, Chen X, Liu S-Y, et al. Elevated expression of VEGF-C and its receptors, VEGFR-2 and VEGFR-3, in patients with mesial temporal lobe epilepsy. J Mol Neurosci. 2016;59(2):241–50.
16. Zhang C-Q, Shu H-F, Yin Q, An N, Xu S-L, Yin J-B, et al. Expression and cellular distribution of vascular endothelial growth factor-C system in cortical tubers of the tuberous sclerosis complex. Brain Pathol. 2012;22(2):205–18.
17. Blümcke I, Thom M, Aronica E, Armstrong DD, Vinters HV, Palmini A, et al. The clinicopathologic spectrum of focal cortical dysplasias: a consensus classification proposed by an ad hoc Task Force of the ILAE Diagnostic Methods Commission. Epilepsia. 2011;52(1):158–74.
18. Campbell SL, Hablitz JJ, Olsen ML. Functional changes in glutamate transporters and astrocyte biophysical properties in a rodent model of focal cortical dysplasia. Front Cell Neurosci. 2014;8:425.
19. Finardi A, Colciaghi F, Castana L, Locatelli D, Marras CE, Nobili P, et al. Long-duration epilepsy affects cell morphology and glutamatergic synapses in type IIB focal cortical dysplasia. Acta Neuropathol. 2013;126(2):219–35.
20. Hynd MR, Lewohl JM, Scott HL, Dodd PR. Biochemical and molecular studies using human autopsy brain tissue. J Neurochem. 2003;85(3):543–62.
21. Issa R, Krupinski J, Bujny T, Kumar S, Kaluza J, Kumar P. Vascular endothelial growth factor and its receptor, KDR, in human brain tissue after ischemic stroke. Lab Invest. 1999;79(4):417–25.
22. Roper SN. In utero irradiation of rats as a model of human cerebrocortical dysgenesis: a review. Epilepsy Res. 1998;32(1–2):63–74.
23. Schwartzkroin PA, Roper SN, Wenzel HJ. Cortical dysplasia and epilepsy: animal models. Adv Exp Med Biol. 2004;548:145–74.
24. Iyer AM, Zurolo E, Boer K, Baayen JC, Giangaspero F, Arcella A, et al. Tissue plasminogen activator and urokinase plasminogen activator in human epileptogenic pathologies. Neuroscience. 2010;167(3):929–45.
25. Myme CIO, Sugino K, Turrigiano GG, Nelson SB. The NMDA-to-AMPA ratio at synapses onto layer 2/3 pyramidal neurons is conserved across prefrontal and visual cortices. J Neurophysiol. 2003;90(2):771–9.

26. Faul F, Erdfelder E, Lang AG, Buchner A. G*Power 3: a flexible statistical power analysis program for the social, behavioral, and biomedical sciences. Behav Res Methods. 2007;39(2):175–91.
27. Sarnat HB. Immunocytochemical markers of neuronal maturation in human diagnostic neuropathology. Cell Tissue Res. 2015;359(1):279–94.
28. Boer K, Troost D, Spliet WGM, van Rijen PC, Gorter JA, Aronica E. Cellular distribution of vascular endothelial growth factor A (VEGFA) and B (VEGFB) and VEGF receptors 1 and 2 in focal cortical dysplasia type IIB. Acta Neuropathol. 2008;115(6):683–96.
29. Ha GE, Cheong E. Spike frequency adaptation in neurons of the central nervous system. Exp Neurobiol. 2017;26(4):179–85.
30. Shinomoto S, Shima K, Tanji J. Differences in spiking patterns among cortical neurons. Neural Comput. 2003;15(12):2823–42.
31. Gomes E, Papa L, Hao T, Rockwell P. The VEGFR2 and PKA pathways converge at MEK/ERK1/2 to promote survival in serum deprived neuronal cells. Mol Cell Biochem. 2007;305(1–2):179–90.
32. Calvo C-F, Fontaine RH, Soueid J, Tammela T, Makinen T, Alfaro-Cervello C, et al. Vascular endothelial growth factor receptor 3 directly regulates murine neurogenesis. Genes Dev. 2011;25(8):831–44.
33. Bain JM, Moore L, Ren Z, Simonishvili S, Levison SW. Vascular endothelial growth factors A and C are induced in the SVZ following neonatal hypoxia-ischemia and exert different effects on neonatal glial progenitors. Transl Stroke Res. 2013;4(2):158–70.
34. Shin Y-J, Park J-M, Cho JM, Cha J-H, Kim SY, Lee M-Y. Induction of vascular endothelial growth factor receptor-3 expression in perivascular cells of the ischemic core following focal cerebral ischemia in rats. Acta Histochem. 2013;115(2):170–7.
35. Wen M-D, Jiang Y, Huang J, Al-Hawwas M, Dan Q-Q, Yang R-A, et al. A novel role of VEGFC in cerebral ischemia with lung injury. Front Neurosci. 2019;13:479.
36. Penco-Campillo M, Comoglio Y, Feliz Morel ÁJ, Hanna R, Durivault J, Leloire M, et al. VEGFC negatively regulates the growth and aggressiveness of medulloblastoma cells. Commun Biol. 2020;3(1):579.
37. Song E, Mao T, Dong H, Boisserand LSB, Antila S, Bosenberg M, et al. VEGF-C-driven lymphatic drainage enables immunosurveillance of brain tumours. Nature. 2020;577(7792):689–94.
38. Zhao H, Hou C, Hou A, Zhu D. Concurrent expression of VEGF-C and neuropilin-2 is correlated with poor prognosis in glioblastoma. Tohoku J Exp Med. 2016;238(2):85–91.
39. Da Mesquita S, Louveau A, Vaccari A, Smirnov I, Cornelison RC, Kingsmore KM, et al. Functional aspects of meningeal lymphatics in ageing and Alzheimer's disease. Nature. 2018;560(7717):185–91.
40. Castañeda-Cabral JL, Beas-Zárate C, Rocha-Arrieta LL, Orozco-Suárez SA, Alonso-Vanegas M, Guevara-Guzmán R, et al. Increased protein expression of VEGF-A, VEGF-B, VEGF-C and their receptors in the temporal neocortex of pharmacoresistant temporal lobe epilepsy patients. J Neuroimmunol. 2019;328:68–72.
41. Zhou F-W, Rani A, Martinez-Diaz H, Foster TC, Roper SN. Altered behavior in experimental cortical dysplasia. Epilepsia. 2011;52(12):2293–303.
42. Zhou F-W, Roper SN. Impaired hippocampal memory function and synaptic plasticity in experimental cortical dysplasia. Epilepsia. 2012;53(5):850–9.
43. Babb TL, Ying Z, Hadam J, Penrod C. Glutamate receptor mechanisms in human epileptic dysplastic cortex. Epilepsy Res. 1998;32(1–2):24–33.
44. Finardi A, Gardoni F, Bassanini S, Lasio G, Cossu M, Tassi L, et al. NMDA receptor composition differs among anatomically diverse malformations of cortical development. J Neuropathol Exp Neurol. 2006;65(9):883–93.
45. Mikuni N, Nishiyama K, Babb TL, Ying Z, Najm I, Okamoto T, et al. Decreased calmodulin-NR1 co-assembly as a mechanism for focal epilepsy in cortical dysplasia. NeuroReport. 1999;10(7):1609–12.
46. Najm IM, Ying Z, Babb T, Mohamed A, Hadam J, LaPresto E, et al. Epileptogenicity correlated with increased N-methyl-D-aspartate receptor subunit NR2A/B in human focal cortical dysplasia. Epilepsia. 2000;41(8):971–6.

SUPPORTING INFORMATION

Additional supporting information may be found in the online version of the article at the publisher's website.

Supplementary Material

FIGURE S1 The immunoreactivity score of VEGF-C, VEGFR-2 and VEGFR-3 in the cortical lesions of FCD patients. Semi-quantitative analysis showed the expression of VEGF-C, VEGFR-2, and VEGFR-3 was increased in the cortical lesions of patients with FCD I, FCD IIa and FCD IIb associated epilepsy. $^{**}p < 0.01$, $^{***}p < 0.001$, unpaired two-tailed *t*-test. $n = 10$-13 specimens in each group

TABLE S1 Clinical and neuropathological characteristics of patients with FCD

TABLE S2 Clinical and neuropathological characteristics of autopsy subjects

TABLE S3 Antibodies used for immunostaining and western blot

TABLE S4 Immunoreactivity scores of VEGF-C, VEGFR-2 and VEGFR-3 in each type of FCD lesions

How to cite this article: Shen K-F, Duan Q-T, Duan W, Xu S-L, An N, Ke Y-Y, et al. Vascular endothelial growth factor-C modulates cortical NMDA receptor activity in cortical lesions of young patients and rat model with focal cortical dysplasia. Brain Pathol. 2022;32:e13065. https://doi.org/10.1111/bpa.13065